Szabolcs Blazsek [a,b], Alvaro Escribano [c,*], and Erzsebet Kristof [d]

Global sea ice volume forecasts for the next 100 years using score-driven threshold climate models

[a] *School of Business, Francisco Marroquín University, Guatemala City, Guatemala*

[b] *Stetson-Hatcher School of Business, Mercer University, Macon, GA, United States*

[c] *Department of Economics, University Carlos III of Madrid, Getafe, Spain*

[d] *Department of Meteorology, Eötvös Loránd University, Budapest, Hungary*

Abstract: The literature on sea ice forecasts uses a variety of general circulation models (GCMs), which suggest diverse forecasts of the date of ice-free Arctic. We use a novel reduced-form time series model, named the score-driven threshold climate model. The advantage of using the novel time series model in comparison with the future simulations of GCMs is that it enables us to forecast based on the assumption that the current trend of climate change continues, while its estimation is easier and less expensive than that of the GCMs. We combine long-run 1-thousand-year frequency climate data for the period of 798 to 1 thousand years ago and short-run annual data from 850 to 2014, by scaling the short-run climate data. We present the evolution of long-run and short-run climate data using descriptive statistical analysis. We estimate the new score-driven threshold climate model using annual data from 850 to 2014 for the global sea ice volume Ice_t and Antarctic land surface temperature Temp_t, from 850 to 2014, for which we use the atmospheric $\text{CO}_{2,t}$ concentration as a clustering variable, to define sub-periods of climate change. We report out-of-sample interval forecasts from 2015 to 2114. We find that if the current trend of climate change continues, then global sea ice will disappear around 2077, and the corresponding mean $\pm$ 2 standard deviation interval forecast is $[2067, 2088]$.

JEL classification: C32, C38, C51, C52, C53, Q54

Keywords: Climate change; global ice volume; atmospheric CO_2; Antarctic land surface temperature; dynamic conditional score; generalized autoregressive score; ice-age models

[*] *Corresponding author.* Address: Department of Economics, University Carlos III of Madrid, Calle Madrid 126, Getafe, 28903, Madrid, Spain. E-mails: blazsek_s@mercer.edu (Blazsek), alvaroe@eco.uc3m.es (Escribano), and ekristof86@staff.elte.hu (Kristof).

1. Introduction

Climate change is the most important global issue on Earth. The influence of humanity on Earth's climate started approximately 10,000 to 15,000 years ago (i.e., the start of the Anthropocene), by commencing agricultural activities such as cultivating plants and livestock (Ruddiman, 2005). That influence significantly increased after the Industrial Revolution (from 1769 to 1840, approximately), and it further increased with an accelerating growth rate during the 20th and 21st centuries. Earth's population rose from 1 billion in 1800 to 8 billion in 2023, which was associated with a significant global-scale economic expansion. One of the consequences is rising global greenhouse gas (GHG) emissions. Compared to the second half of the 19th century, the global land surface temperature for the end of the 21st century is very likely to rise by 1.0 to 1.8 °C under the "very low GHG emissions scenario", by 2.1 to 3.5 °C for the "intermediate GHG emissions scenario", and by 3.3 to 5.7 °C under the worst-case scenario, "very high GHG emissions scenario" (IPCC, 2021). The latter scenario implies dramatic consequences on nature and wildlife in terrestrial, wetland, and ocean ecosystems, and on humanity concerning food and water security, migration, health, higher risk of conflict worldwide, reduction of global economic product, and a possible collapse of the current societal organization (IPCC, 2021).

In this paper, we focus on using the score-driven threshold climate model to assess the possibility of ice-free Oceans at the global level, by forecasting global sea ice volume until the year 2114. Several works in the literature focus on predicting sea ice volume for the Arctic Ocean. Based on the simulation results of a general circulation model (GCM), Holland, Bitz, and Tremblay (2006) predict near-ice-free September conditions for the Arctic Ocean by the year 2040. Boé, Hall, and Qu (2009), use CIMP3 (Coupled Model Intercomparison Project, CMIP, Phase 3) GCMs and predict the ice-free Arctic Ocean around the year 2100, under the assumption of medium future GHG emissions. Wang and Overland (2009) use alternative CMIP3 GCMs and predict the nearly ice-free Arctic Ocean for 2037. Wang and Overland (2012) update those forecasts for CMIP5 (CMIP, Phase 5) and predict the nearly ice-free Arctic Ocean around September 2035, under the highest GHG emission scenario. Stroeve et al. (2012), use

CMIP3 models and, under a lower GHG emissions scenario, predict that the ice-free Arctic Ocean after 2100 and ice-free conditions in 2045 within one standard deviation of the mean. However, they find that turning to the end of the 21st century, the CMIP5 multi-model ensemble mean never reaches ice-free conditions. IPCC (2014) predicts an ice-free Arctic summer around 2050, under the scenario of the highest possible GHG emissions. That forecast is updated by IPCC (2021) which reports that the Arctic Ocean will likely become practically ice-free in September before the year 2050 under all Shared Socioeconomic Pathway (SSP) scenarios. Melillo et al. (2014) report that the Arctic Ocean is expected to be ice-free in summer by the 2030s, and the subsequent report of USGCRP (2018) (US Global Change Research Program, USGCRP) predicts the ice-free Arctic Ocean around 2050.

The work of Guarino et al. (2020) predicts that summer sea ice floating on the surface of the Arctic Ocean could disappear entirely by 2035. Guarino et al. (2020) also present a summary of forecasting results for alternative climate models, according to which multi-model CMIP3 to CMIP6 the mean predictions with ranges for a summer sea ice-free Arctic are (i) the year 2062 with [2040,2086] for CMIP3, (ii) the year 2048 with [2020,2081] for CMIP5, and (iii) the year 2046 with [2029,2066] for CMIP6. We note that the latest year of sea ice disappearance for CMIP6 models is 2066 and that 50% of the models predict sea ice-free conditions between the years 2030 and 2040. In recent work, Docquier and Koenigk (2021) show that the CMIP6 (CMIP, Phase 6) models which perform the best at simulating Arctic sea ice trends, project the first ice-free conditions around 2035 under SSP5-8.5, which is the SSP scenario of continually accelerating GHG emissions meaning a fossil-fueled development (O'Neill et al., 2016). The work of Diebold et al. (2022) reports point, interval, and density forecasts of the area, extent, thickness, and volume of Arctic sea ice. Those authors impose the joint constraint for these measures, according to which they simultaneously arrive at an ice-free Arctic sea. They apply this forecasting procedure to carbon-trend models of sea ice and atmospheric CO_2 concentration and time-trend models of sea ice and time. The resulting forecasts are mutually consistent and predict a nearly ice-free Arctic summer by the mid-2030s with an 80% probability.

We contribute to the literature by updating the recent score-driven threshold ice-age model of Blazsek and Escribano (2023). In the work of Blazsek and Escribano (2022), the score-driven ice-age model is introduced, and it is shown that the statistical performance of that model is superior to the statistical performance of the ice-age model of Castle and Hendry (2020). Blazsek and Escribano (2022) also show that the forecasting performances of both models are similar and not very effective for the climate variables for the Anthropocene. Motivated by that result, Blazsek and Escribano (2023) introduce the score-driven threshold ice-age model. Those authors use the same data for climate and orbital variables for the last 798-thousand-year period as Castle and Hendry (2020) and Blazsek and Escribano (2022), and they forecast global ice volume, atmospheric CO_2, and Antarctic land surface temperature for the last 100,000 years of the sample (i.e., in-sample forecasts) and the forthcoming 5,000 years (i.e., out-of-sample forecasts). Blazsek and Escribano (2023) use Ward's linkage clustering procedure (Ward, 1963), to define sub-periods of climate change. The score-driven threshold ice-age model improves the forecasting performances of the models of Castle and Hendry (2020) and Blazsek and Escribano (2022). Nevertheless, Blazsek and Escribano (2023) use 1-thousand-year frequency observations, which does not allow the measurement of climate effects of humanity for the last 250 years with unprecedented high levels of $CO_{2,t}$ and Temp_t, and unprecedented low levels of Ice_t.

We perform an extensive model selection analysis to find the optimal score-driven model specification, which we name the score-driven threshold climate model. We present the technical details of the score-driven threshold climate model specification and its statistical inference. We combine long-run 1-thousand-year frequency climate data for the period of 798 to 1 thousand years ago and short-run annual data from 850 to 2014, by scaling short-run climate data to long-run climate data. To study what would have happened to global ice volume if GHG emissions had stopped, we perform in-sample forecasting analysis using the estimation windows 850 to 1906 and 850 to 1979. The in-sample forecasts indicate that observed Ice_t is below the forecast interval after 2001 and observed Temp_t is above the forecast interval from the mid-1990s. According to these in-sample forecasts, Ice_t would not disappear in the forthcoming

decades. Finally, we estimate the model for the dependent variables Ice_t and Temp_t, and we report out-of-sample forecasts for the period of 2015 to 2114. We find that if the current trend of climate change continues, then all global sea ice will disappear around the year 2077, and the corresponding mean $\pm$ 2 standard deviation interval forecast is $[2067, 2088]$.

The remainder of this paper is organized as follows: Section 2 describes the data. Section 3 presents the time series methods. Section 4 presents the empirical results. Section 5 concludes.

2. Data

In this section, we describe the data for the climate models of this paper. We use long-run and short-run climate data on global ice volume, Antarctic land surface temperature, and atmospheric CO_2 concentration. The long-run climate data is from 798 to 1 thousand years ago. The short-run climate data is for the period of the year 850 to the year 2014. Long-run and short-run climate data are combined by scaling the measures of the short-run variables to the measures of the long-run variables. We provide a descriptive statistical analysis for all variables.

2.1. Long-run climate data

For the long-run climate data, the variables are global sea ice volume Ice_t, Antarctic land surface temperature Temp_t, and atmospheric $\text{CO}_{2,t}$ concentration, which are observed with a 1-thousand-year observation frequency. These data are also used in the works of Castle and Hendry (2020) and Blazsek and Escribano (2022, 2023). The data source of global sea ice volume Ice_t is the work of Lisiecki and Raymo (2005), in which time series of the $\delta^{18}\text{O}$, obtained from calcium carbonate (CaCO_3) shells of foraminifera, are used to approximate temperature. Those authors use benthic records of foraminifera from seafloor sediment, which were collected at 57 globally distributed sites. Those sites are well-distributed in latitude, longitude, and depth in the Atlantic, Pacific, and Indian Oceans. The data source of Antarctic land surface temperature Temp_t is the work of Jouzel et al. (2007), in which temperature data were obtained within the European Project for Ice Coring in Antarctica (EPICA) at the Concordia Station (Dome C), by using deuterium $\delta\text{D}_{\text{ice}}$ measurements from the surface down to 3,259.7 meters.

Within the EPICA, two deep ice cores have been drilled at Kohnen Station and Concordia Station (Dome C). The drillings were stopped at or a few meters above bedrock at a depth of 2,774 meters and 3,270 meters, respectively. The data source of atmospheric $CO_{2,t}$ is the work of Lüthi et al. (2008), in which changes in past atmospheric CO_2 concentrations are determined by measuring the composition of air trapped in ice cores from EPICA.

Castle and Hendry (2020) and Blazsek and Escribano (2022, 2023) also use the following variables as explanatory variables in the ice-age models: (i) eccentricity of Earth's orbit Ec_t, (ii) obliquity of Earth's rotational axis relative to the ecliptic Ob_t, and (iii) precession of the equinox Pr_t. We omit these variables since our main focus is the analysis of the more recent period of 850 to 2014, for which these orbital variables show smooth linear trends. Moreover, motivated by the work of Blazsek and Escribano (2022), we also omit the following explanatory variables: (i) the variations in the Sun's radiation output, (ii) volcanic eruption particles in the atmosphere and ice cover, and (iii) changes in the Earth's magnetic poles.

2.2. Short-run climate data

The short-run climate data, with an annual observation frequency, are for the period of 850 to 2014, for which we use global sea ice volume Ice_t and Antarctic land surface temperature Temp_t, obtained from the GCMI MRI-ESM2.0 (Meteorological Research Institute Earth System Model Version 2.0), because of its high temporal resolution. The data are from GCM MRI-ESM2.0 (Yukimoto et al., 2019, 2020), which is disseminated by CMIP6 (Eyring et al., 2016) that is part of the Paleoclimate Modelling Intercomparison Project, Phase 4 (PMIP4; Jungclaus et al., 2017). In the case of the MRI-ESM2.0, the experiment r1i1p1f1 was used. We also use data on atmospheric CO_2 concentration for the same period, to cluster the Ice_t and Temp_t time series into sub-periods. The source of the $CO_{2,t}$ data is the work of Meinshausen et al. (2017). We note that 2014 is the most recent date for which historical annual climate data are available for us. We use these data sources for Ice_t, Temp_t, and $CO_{2,t}$, because these are the only sources from which annual data for the period of 850 to 2014 are available for us.

Three comments about the short-run dataset: (i) Although according to the Supplementary Material of Docquier and Koenigk (2021), GCM MRI-ESM2.0 is not among the GCMs which performed the best at simulating Arctic sea ice trends, we use this GCM due to the availability of global ice volume data for the last 1 thousand years in MRI-ESM2.0. In the work of Jungclaus et al. (2017), methods were applied to the 'past1000' simulation results for the period of 850 to 1849, and the historical simulation results for the period of 1850 to 2014. GHG concentrations for the 'past1000' are consistent with the historical CMIP6 simulations, and are also consistent with observations (Jungclaus et al., 2017). (ii) Jungclaus et al. (2017) note that during the second half of the 9th century, there was a relatively calm climate period when no glaring changes occurred to the natural constraints, e.g., regarding volcanism and solar activity, it is also quite far from the medieval climate anomaly (MCA) between 950 and 1250. This motivates the start year of the second sample of the present paper. (iii) The GHG concentration data of this paper is a standard dataset, which is part of input4MIPs (input datasets for Model Intercomparison Projects) (see at the following website: https://esgf-node.llnl.gov/projects/input4mips/), that serves as input for all GCMs in CMIP6 in the literature.

2.3. Scaling of climate variables, descriptive analysis

We combine the long-run and short-run climate datasets of Table 1(a)-(b), respectively, by scaling the measures of the shot-run climate variables of Table 1(b) to the measures of the long-run climate variables of Table 1(a). Scaling for one of the variables is done as follows. We denote global ice volume from 798 to 1 thousand years ago by $\tilde{\text{Ice}}_t$ and we denote global ice volume from 1014 to 2014 by Ice^*_t. Then, we scale global ice volume Ice^*_t for $t = 1014, \ldots, 2014$, by using $\text{Ice}^*_{1014} \times (\tilde{\text{Ice}}_{1014}/\text{Ice}^*_{1014})$. Hence, we use the same measurements in Table 1(a)-(b).

In Table 1(a), Ice_t, Temp_t, and $\text{CO}_{2,t}$ for the long-run climate data are presented. This table shows the definitions of variables, observation period, units of measurement, data sources, and some descriptive statistics for each variable. An important descriptive statistic is the Jarque–Bera test (Jarque and Bera, 1980) of normal distribution under H_0, for which the null hypothesis

of normal distribution of each dependent variable is rejected at the 1% level of significance.

In Table 1(b), Ice_t, Temp_t, and $\text{CO}_{2,t}$ for the short-run climate data are presented. This table shows the definitions of variables, observation period, units of measurement, data sources, and some descriptive statistics for each variable. We also present the Jarque–Bera test, for which the null hypothesis of normal distribution of Ice_t and $\text{CO}_{2,t}$ is rejected at the 1% level of significance.

Moreover, in Fig. 1, we present the evolution of Ice_t, Temp_t, and $\text{CO}_{2,t}$ for the period of 798 thousand years ago to the year 2014. In Fig. 2, we present the evolution and forecasts of Ice_t and Temp_t for the period of 798 thousand years ago to the year 2114, as we forecast Ice_t and Temp_t using the score-driven threshold climate model in this paper. In Fig. 3, we present the evolution of Ice_t, Temp_t, and $\text{CO}_{2,t}$ for the period of 850 to 2014.

Finally, in Fig. 4(a)-(b), we present the evolution of Ice_t and Temp_t and their smoothed signals, i.e., $E(\text{Ice}_t|\text{Ice}_1, \ldots, \text{Ice}_T)$ and $E(\text{Temp}_t|\text{Temp}_1, \ldots, \text{Temp}_T)$, respectively, from 850 to 2014. The smoothed signals are estimated by using the score-driven methods of Blazsek, Ayala, and Licht (2022), by using the following score-driven quasi-autoregressive (QAR) model:

$$y_t = \mu_t = \exp(\lambda)\epsilon_t \tag{1}$$

$$\mu_t = \phi\mu_{t-1} + \psi u_{t-1} \tag{2}$$

$$u_t = \frac{\nu \exp(\lambda)\epsilon_t}{\nu + \epsilon_t^2} \tag{3}$$

where y_t is either Ice_t or Temp_t, and $\epsilon_t \sim t(\nu)$ is an i.i.d. error term. The parameter estimates and model diagnostics for this model are presented in Table 1(c)-(d), respectively.

Figs. 1, 2, 3, and 4(a)-(b) indicate the significant influence of humanity on Ice_t and $\text{CO}_{2,t}$. In particular, Figs. 1(a) and 1(c) show the significant influence of humanity on Ice_t and $\text{CO}_{2,t}$, respectively, by showing the significant recent decrease in Ice_t and increase in $\text{CO}_{2,t}$, respectively. A similar decreasing effect on Ice_t is shown in Fig. 2(a). Furthermore, Figs. 3(a) and 3(c) also show the significant negative and positive influence of humanity on Ice_t and $\text{CO}_{2,t}$, respectively. Finally, we also highlight the negative effect of humanity on Ice_t in Fig. 4(a).

3. Methods

In this section, we present the clustering methods that we use to identify structural changes in climate variables, and we also present the score-driven threshold climate model.

3.1. Clustering of climate variables

We cluster Ice_t and Temp_t by using $\text{CO}_{2,t}$ with Ward's linkage clustering method (Ward, 1963). The use of Ward's clustering method to specify the score-driven threshold climate model is motivated by the resulting impressive forecasting performance for climate variables, as shown in the work of Blazsek and Escribano (2023). Many of the standard clustering methods are special cases of this general clustering method. Ward's clustering method identifies the different historical periods of abrupt climate changes (periods of structural changes). For Ward's clustering, we initially set the final number of groups we would like to create. In this paper, using $\text{CO}_{2,t}$ observations, we studied the performances of 2 to 5 groups. Initial statistical analysis suggested that clustering to 3 groups is superior to the alternatives for the period of 850 to 2014.

Ward's linkage clustering method is an agglomerative (i.e., bottom-up) hierarchical clustering method, which begins with each observation being considered as a separate group (i.e., T groups each of size 1). Then, the closest two groups are combined (i.e., $T-1$ groups, one of size 2 and the rest of size 1). To decide which clusters should be combined, a measure of dissimilarity (i.e., linkage criterion) between sets of observations is required. Ward suggested that the linkage criterion for choosing the pair of clusters to merge at each step is based on the optimal value of an objective function. Ward's method joins the two groups that result in the minimum increase in the error sum of squares (ESS). It can be interpreted as forming hierarchical combinations of pairs of clusters that minimize the increase in information loss, as measured by an increase in ESS, at each step (Everitt, 1993). This process creates a hierarchy of clusters, and it continues until all observations belong to the same group. In the chosen clustering procedure, we stop the process of combination of groups when all observations belong to 3 groups, which are the periods of (i) 850 to 1906, (ii) 1907 to 1979, and (iii) 1980 to 2014.

3.2. Score-driven threshold climate model

We start with a brief review of score-driven models. Score-driven time series models are introduced in the works of Creal, Koopman, and Lucas (2008) and Harvey and Chakravarty (2008). Those authors name the score-driven models generalized autoregressive score (GAS) and dynamic conditional score (DCS) models, respectively. Score-driven models are observation-driven time series models (Cox, 1981), in which the filters are updated using the scaled conditional score functions of the log-likelihood (LL) of the dependent variables. Score-driven models are estimated by using the maximum likelihood (ML) method (Harvey, 2013; Blasques et al., 2022).

Some of the statistical advantages of the score-driven models are the following. (i) The updating mechanisms of those models are generalizations of those of the classical time series models, e.g., ARMA (autoregressive moving average) (Box and Jenkins, 1970), GARCH (generalized autoregressive conditional heteroskedasticity) (Engle, 1982; Bollerslev, 1986), and VARMA (vector ARMA) (Tiao and Tsay, 1989). (ii) Score-driven models are robust to outliers (Harvey, 2013; Blazsek and Escribano, 2016a, 2016b, 2022; Ayala, Blazsek, and Escribano, 2022). (iii) A score-driven update locally reduces the Kullback–Leibler distance between the true and estimated values of the score-driven filter in every step, and only score-driven models have this property (Blasques, Koopman, and Lucas, 2015). In other words, score-driven filters use an information-theoretically optimal updating mechanism. (iv) Score-driven updates also satisfy stronger optimality properties, based on a global definition of Kullback–Leibler divergence (Lauria, 2021). Score-driven updates reduce the distance between the expected updated parameter and the pseudo-true parameter. Depending on the conditional density and the scaling of the score, the optimality result can hold globally over the parameter space (Lauria, 2021).

We note that the linear updating mechanisms of ARMA and VARMA, and the quadratic updating mechanism of GARCH are optimal from an information-theoretic perspective only if the data-generating process (DGP) has a normal distribution. According to the descriptive statistics, the DGPs of climate variables are not normal distributions (Table 1), and there are important shifts in the levels of those variables (Figs. 1 to 4(a)-(b)) which indicate the presence

of outliers in the dataset. Therefore, advantages (i) to (iv) may imply improvements in statistical inferences when score-driven models are applied to the climate data.

In the work of Castle and Hendry (2020), estimation and forecasting results are presented for a general unrestricted model (GUM), named the ice-age model. In the work of Blazsek and Escribano (2022), the score-driven ice-age model is introduced, and they show that the statistical performance of their model is superior to that of the ice-age model of Castle and Hendry (2020). The works of Castle and Hendry (2020) and Blazsek and Escribano (2022) use data for the first 698 thousand years of the sample, for which humanity did not influence the Earth's climate, forecast the Antarctic ice volume, atmospheric CO_2, and land surface temperature for the last 100 thousand years of the sample. For the last 10 to 15 thousand years, when human activity could have influenced the Earth's climate, they find that (i) the forecasts of ice volume are above the observed ice volume, (ii) the forecasts of the atmospheric CO_2 level are below the observed CO_2 level, and (iii) the forecasts of temperature are below the observed temperature.

One possible interpretation of the imprecise climate forecasts of those models is the structural change in the parameters of the models generated by human activity during the Anthropocene period. However, if the climate models naturally produce structural changes in the parameters of the models due to changes in the reactions to the evolution of orbital variables (e.g., eccentricity, obliquity, and precession), then we cannot only associate those imprecise climate forecasts with the impact of human activity.

To address this issue, Blazsek and Escribano (2023) model structural changes explicitly, using ice-age models with time-varying parameters based on clusters formed by threshold values of $CO_{2,t}$, Temp_t, and Ice_t for the period of 798 to 1 thousand years ago. Those authors show that, once we control for all structural changes, the models forecast well out-of-sample during the last 10 to 15 thousand years. Clearly, human activity is one of the main factors generating recent structural changes in the climate models, but it is not the unique factor over longer periods (identification problem). The in-sample forecasting performances of the models of Castle and Hendry (2020) and Blazsek and Escribano (2022) are significantly improved over the last 100

thousand years, using the training window of 798 to 101 thousand years ago.

The results in the works of Castle and Hendry (2020) and Blazsek and Escribano (2022, 2023) are based on data with high temporal aggregation. Each observation represents values over 1 thousand years and is not appropriate to evaluate the significant impact of human activity on climate change since the Industrial Revolution. In the score-driven Markov-switching models of Blazsek and Escribano (2023), asymmetries generated by periods of high CO_2 levels and rapid increases in CO_2 are found. Therefore, in the present paper, we use annual data from 850 to 2014 for a new score-driven threshold climate model. The structural changes are generated by high increases in the levels of CO_2 and estimated using cluster analysis. We identify two threshold values of CO_2 corresponding with the years 1906 and 1979, see Fig. 3(c). For our dataset, the fast increase in the levels of CO_2 is clearly generated by economic growth based on the increasing use of fossil fuels, with highly concentrated cities of increasing population. Therefore, in this paper, we solve the previous identification issue of the sources of structural changes during the Anthropocene. The identification of climate changes is clearer in the short run because, during a short time span period, the orbital variables are smoothly evolving and do not strongly affect the parameters of the climate models of temperature and volume of ice.

To find the best score-driven climate specification, we perform an extensive model selection procedure that starts with using the full specification of the score-driven threshold ice-age model of Blazsek and Escribano (2023). Model selection is performed using annual data for the period of 850 to 2014, and we use 2 to 5 alternative numbers of periods for clustering. We start with the dependent variables $y_t = (\text{Ice}_t, \text{CO}_{2,t}, \text{Temp}_t)'$. We also consider the first and second differences of $\text{CO}_{2,t}$ as alternatives. Nevertheless, due to the explosive and exponentially upward trending behavior of $\text{CO}_{2,t}$, we decided to use $\text{CO}_{2,t}$ as a clustering variable. Therefore, the score-driven threshold climate model reported in this paper is specified for $y_t = (\text{Ice}_t, \text{Temp}_t)'$ as follows:

$$y_t = \delta_t + \mu_t + v_t \tag{4}$$

$$\delta_t = \alpha(1)D_{1,t} + \beta(1)T_{1,t} + \alpha(2)D_{2,t} + \beta(2)T_{2,t} + \alpha(3)D_{3,t} + \beta(3)T_{3,t} \tag{5}$$

$$\mu_t = [\Gamma(1)D_{1,t} + \Gamma(2)D_{2,t} + \Gamma(3)D_{3,t}]\mu_{t-1} + [\Psi(1)D_{1,t} + \Psi(2)D_{2,t} + \Psi(3)D_{3,t}]u_{t-1} \tag{6}$$

$$v_t \sim t_3[0, \Omega(1)\Omega(1)'D_{1,t} + \Omega(2)\Omega(2)'D_{2,t} + \Omega(3)\Omega(3)'D_{3,t}, \nu] \tag{7}$$

for $t = 1, \ldots, T$. The conditional mean of y_t, conditional on $\mathcal{F}_t = (y_1, \ldots, y_{t-1}, \mu_1)$ is $(\delta_t + \mu_t)$. The reduced-form error term for sub-period $i = 1, 2, 3$ is $v_t \sim t_2[0, \Sigma(i), \nu]$ with a bivariate i.i.d. t-distribution (t_2 indicates two-dimensional t-distribution), where the scale matrix is $\Sigma(i) \equiv \Omega(i)\Omega'(i)$ (2×2), for which $\Omega(i)$ (2×2) is a lower-triangular squared matrix with positive elements in the diagonal, and $\nu > 0$ is the degrees of freedom parameter. We note that the use of the common degrees of freedom parameter for the three sub-periods is due to the results of the aforementioned model selection procedure. The remaining parameters are specified as follows: $\alpha(i)$ and $\beta(i)$ for $i = 1, 2, 3$ are 2×1 vectors; $\Gamma(i)$ and $\Psi(i)$ for $i = 1, 2, 3$ are 2×2 diagonal matrices. We also note that the use of the diagonal $\Gamma(i)$ and $\Psi(i)$ is also due to the results of the aforementioned model selection procedure.

The linear time trend with structural changes is modeled as follows: $D_{1,t} = 1$ for $t \leq T_{1B}$ and zero otherwise, $D_{2,t} = 1$ for $T_{1B} < t \leq T_{2B}$ and zero otherwise, $D_{3,t} = 1$ for $t > T_{2B}$ and zero otherwise, $T_{1,t} = t$ for $t \leq T_{1B}$ and zero otherwise, $T_{2,t} = t - T_{1,t}$ for $T_{1B} < t \leq T_{2B}$ and zero otherwise, and $T_{3,t} = t - T_{2,t}$ for $t > T_{2B}$ and zero otherwise. In these definitions, the dates of structural changes, T_{1B} and T_{2B}, are determined using Ward's linkage clustering method for $\mathrm{CO}_{2,t}$. In our empirical application, we find that $T_{1B} = 1906$ and $T_{2B} = 1979$.

The 2×1 scaled score function u_t is defined as follows. The log conditional density of y_t is:

$$\ln f(y_t|\mathcal{F}_{t-1}; \Theta) = \ln \Gamma\left(\frac{\nu+2}{2}\right) - \ln \Gamma\left(\frac{\nu}{2}\right) - \ln(\pi\nu) - \frac{1}{2}\ln|\Sigma(i)| - \frac{\nu+2}{2}\ln\left[1 + \frac{v_t'\Sigma(i)^{-1}v_t}{\nu}\right] \tag{8}$$

where $v_t = y_t - \delta_t - \mu_t$, $\Theta = (\Theta_1, \ldots, \Theta_S)'$ is the vector of time-invariant parameters. The partial

derivative of the log conditional density $\ln f(y_t|\mathcal{F}_{t-1};\Theta)$ with respect to $(\delta_t + \mu_t)$ is:

$$\frac{\partial \ln f(y_t|\mathcal{F}_{t-1};\Theta)}{\partial(\delta_t+\mu_t)} = \frac{\nu+2}{\nu}\Sigma(i)^{-1} \times \left(1 + \frac{v_t'\Sigma(i)^{-1}v_t}{\nu}\right)^{-1} v_t \equiv \frac{\nu+2}{\nu}\Sigma(i)^{-1} \times u_t \tag{9}$$

The scaled score function u_t is defined in the second equality of Equation (9), where v_t is multiplied by $\{1 + [v_t'\Sigma(i)^{-1}v_t]/\nu\}^{-1} = \nu/[\nu + v_t'\Sigma(i)^{-1}v_t] \in (0,1)$. Hence, the scaled score function is bounded by the reduced-form error term: $|u_t| < |v_t|$. All elements of u_t are bounded functions of v_t for $\nu < \infty$ (Harvey, 2013), and all moments of u_t are well-defined. In the work of Harvey (2013), it is shown that u_t is multivariate i.i.d. with mean zero and a covariance matrix:

$$\text{Var}(u_t) = E\left[\frac{\partial \ln f(y_t|\mathcal{F}_{t-1};\Theta)}{\partial \mu_t} \times \frac{\partial \ln f(y_t|\mathcal{F}_{t-1};\Theta)}{\partial \mu_t'}\right] = \frac{\nu+2}{\nu+4} \times \Sigma(i)^{-1} \tag{10}$$

for the climate sub-periods $i = 1, 2, 3$.

Finally, the variance of the reduced-form error term is factorized, as follows:

$$\text{Var}(v_t) = \Sigma(i) \times \frac{\nu}{\nu-2} = \left(\frac{\nu}{\nu-2}\right)^{1/2} \times \Omega(i)\Omega'(i) \times \left(\frac{\nu}{\nu-2}\right)^{1/2} \tag{11}$$

Based on that, the following multivariate i.i.d. structural-form error term ϵ_t is introduced:

$$v_t = \left(\frac{\nu}{\nu-2}\right)^{1/2} \Omega(i) \times \epsilon_t \tag{12}$$

where $E(\epsilon_t) = 0$, $\text{Var}(\epsilon_t) = I_2$ and $\epsilon_t \sim t_2[0, I_2 \times (\nu-2)/\nu, \nu]$. In Fig. 5, we present u_t as a function of the structural-form error term ϵ_t for the most recent sub-period of 1980 to 2014. The figure presents u_t for the estimates for the score-driven threshold climate model. In the three-dimensional graphs of Fig. 5, we present the elements of u_t as functions of $\epsilon_{1,t}$ and $\epsilon_{2,t}$. In each panel of Fig. 5, maximum and minimum points can be observed for u_t as a function of ϵ_t, which are by the result that u_t converges in probability to zero as any of its arguments ϵ_t go to infinity, i.e., extreme values of ϵ_t are discounted by u_t. Therefore, Fig. 5 indicates that the

score-driven threshold climate model is robust to extreme observations.

We estimate the score-driven threshold climate model for the climate data in two steps. In the first step, we estimate the parameters of the linear trend model with structural changes, i.e., $\alpha(i)$ and β_i for $i = 1, 2, 3$, by using the OLS-HAC (ordinary least squares; heteroskedasticity and autocorrelation consistent) method (Newey and West, 1987). We substitute those parameter estimates for the second step, in which the remaining parameters are estimated by using the ML method (Harvey, 2013; Blasques et al., 2022).

We note that for in-sample forecasting analysis, involving reduced estimation windows, we also use climate models for the period of 850 to 1979 with one structural change in 1906.

4. Empirical results

In this section, we summarize the empirical results for the score-driven threshold climate model.

In Table 2(a), we present the parameter estimates for the linear trend model with structural changes. In Table 2(b), we present the parameter estimates and model diagnostics for the score-driven threshold climate model. Concerning model diagnostics, all statistics support the use of the score-driven threshold climate specification. (i) The maximum modulus of the eigenvalues of $\Gamma(i)$ for $i = 1, 2, 3$, denoted by $C(i)$ in Table 2(b), indicate that the score-driven filter μ_t is asymptotically covariance stationary. In Fig. 4(c)-(d), we present the estimates of μ_t. (ii) The Escanciano–Lobato test (Escanciano and Lobato, 2009) suggests that the structural-form errors, $v_{1,t}$ and $v_{2,t}$, are martingale difference sequences (MDS). The same test also suggests that the scaled score functions, $u_{1,t}$ and $u_{2,t}$, are MDS. (iii) The Ljung–Box test (Ljung and Box, 1978) suggests that the structural-form errors, $v_{1,t}$ and $v_{2,t}$, are independent time series. The same test also suggests that the scaled score functions, $u_{1,t}$ and $u_{2,t}$, are independent time series. In Fig. 6, we present the estimates of v_t and u_t.

In Fig. 7, we study the in-sample forecasts of Ice_t and Temp_t for the period of 1980 to 2014. For the forecasting period 1980 to 2014 (Fig. 7(a)-(b)), we use a score-driven climate model with one structural change in the year 1906, which defines the periods 850 to 1906 and 1907 to 1979.

In this way, we approximate what would have happened with the evolution of Ice_t and Temp_t, if GHG emissions would not have increased further. The corresponding parameter estimates and model diagnostics are presented in Table 3, in which the model diagnostics support the specification of the score-driven climate model with one structural change. In Fig. 7(a), the lower bound of Ice_t forecasts is higher than the observed value of Ice_t after 2001. Moreover, in Fig. 7(b), the upper bound of Temp_t tends to be lower than the observed value of Temp_t from the mid-1990s. According to these results, Ice_t would not disappear in the forthcoming decades.

Using the estimates of the score-driven threshold climate model, we perform out-of-sample forecasting from 2015 to 2114. In Fig. 8(a)-(b), we present the evolution and forecasts of Ice_t and Temp_t, respectively, for the period of 850 to 2114. In Fig. 8(c)-(d), we present the evolution and forecasts of Ice_t and Temp_t, respectively, for the period of 1980 to 2114. Fig. 8 indicates that if the current trend of climate change continues, then all global sea ice will disappear around the year 2077, and the corresponding mean $\pm$ 2 standard deviation interval forecast is $[2067, 2088]$.

5. Discussion

In the work of Blazsek and Escribano (2022), a time series model, named the score-driven ice-age model, is introduced. Recently, the statistical modeling of climate variables has remained popular in the field of climatology. For example, Ahn et al. (2022) use autoregressive moving average (ARIMA) models to examine sea ice concentration in the region of the Barents and Kara Seas. Wu et al. (2023) use ARIMA models to analyze and forecast the sea ice concentration along a shipping route in the Northern Sea. Brennan et al. (2023) use linear inverse models (LIMs) to predict, among others, Arctic sea ice concentration and thickness.

The statistical modeling of climate variables, which is performed in the present paper, has gained popularity since statistical models are computationally less expensive compared to the dynamic models, i.e. GCMs, which require a significant amount of data (Wu et al., 2023). Moreover, based on the analysis of Stroeve et al. (2014), the forecasting performance of statistical models is slightly higher than the forecasting performance of dynamic models (Blanchard-

Wrigglesworth et al., 2017; Brennan et al., 2023). The uncertainty and initial conditions of dynamic models are partly responsible for that (Blanchard-Wrigglesworth et al., 2015, 2017). Andersson et al. (2021) introduce a deep learning-based Arctic sea ice forecasting system, which also outperforms a state-of-the-art dynamic model. Furthermore, temporally varying relationships between climate variables and climate factors can also be examined through statistical modeling (Ahn et al., 2014).

It is shown that the statistical performance of the score-driven ice-age model is superior to the statistical performance of the ice-age model of Castle and Hendry (2020). Blazsek and Escribano (2022) also show that the forecasting performances of both models are similar and not very effective for the climate variables for the Anthropocene. Motivated by that result, Blazsek and Escribano (2023) introduce the score-driven threshold ice-age model. Those authors use the same data for climate and orbital variables for the last 798-thousand-year period as Castle and Hendry (2020) and Blazsek and Escribano (2022), and they forecast global ice volume, atmospheric CO2, and Antarctic land surface temperature for the last 100,000 years of the sample (i.e., in-sample forecasts) and the forthcoming 5,000 years (i.e., out-of-sample forecasts). Blazsek and Escribano (2023) use Ward's linkage clustering procedure (Ward, 1963), to define sub-periods of climate change. The score-driven threshold ice-age model improves the forecasting performances of the models of Castle and Hendry (2020) and Blazsek and Escribano (2022). Nevertheless, Blazsek and Escribano (2023) use 1-thousand-year frequency observations, which does not allow the measurement of climate effects of humanity for the last 250 years with unprecedented high levels of $CO_{2,t}$ and Temp_t, and unprecedented low levels of Ice_t.

The results of the present paper suggest that the proposed score-driven climate model is suitable for forecasting the evolution of global sea ice volume.

6. Conclusions

In this paper, we have used a novel climate time series specification, named the score-driven threshold climate model. As an example, we presented its usage, and interval forecasts of global

sea ice volume until the year 2114, to study the first date of ice-free Oceans on Earth. There is significant literature on sea ice forecasts for the Arctic Ocean, using a variety of climate models for CMIP3, CMIP5, and CMIP6, which suggest diverse forecasts for the first date of an ice-free Arctic Ocean. The advantage of using the novel time series model in comparison with the future simulations of GCMs is that it enables us to predict the future based on the assumption that the current trend of climate change continues, while its estimation is more straightforward and less expensive than that of the GCMs. Furthermore, it can be used for statistical downscaling.

The score-driven threshold climate model can be used to define sub-periods of climate change. We have combined long-run 1-thousand-year frequency climate data for the period of 798 to 1 thousand years ago and short-run annual data from 850 to 2014, by scaling the short-run climate data. We have compared the evolution of long-run and short-run climate data using descriptive statistical analysis. We have reported estimations for the period of 850 to 2014 for global sea ice volume Ice_t and Antarctic land surface temperature Temp_t, for which we have used the atmospheric $\text{CO}_{2,t}$ concentration as a clustering variable. We have performed an extensive model selection procedure, to find the optimal score-driven model specification. For the score-driven threshold climate model, we have used Ward's clustering with the clustering variable $\text{CO}_{2,t}$, which has defined 3 sub-periods of climate change for Ice_t and Temp_t: (i) 850 to 1906, (ii) 1907 to 1979, and (iii) 1980 to 2014. We have estimated the model for the dependent variables Ice_t and Temp_t, and we have reported out-of-sample interval forecasts for the period of 2015 to 2114.

We have presented interval forecasts of global sea ice volume until the year 2114, to study the first date of ice-free Oceans on Earth. There is significant literature on sea ice forecasts for the Arctic Ocean, using a variety of GCMs for CMIP3, CMIP5, and CMIP6, which suggest diverse forecasts for the first date of an ice-free Arctic Ocean. We have taken a global perspective on sea ice forecasting, and we have used a novel climate time series specification, named the score-driven threshold climate model. The advantage of using the novel time series model in comparison with the future simulations of GCMs is that it enables us to predict the future based on the assumption that the current trend of climate change continues, while its estimation is

more straightforward and less expensive than that of the GCMs.

For the in-sample forecasts from 1980 to 2014, we estimated our score-driven threshold climate model with one structural change for the period of 850 to 1979. The in-sample multi-step ahead forecasts predict decreasing values of ice volume but still within the 95% confidence bands until the early 2000 years. However, after the early 2000 years, the ice-volume forecast continued to decrease, and since then the values of the ice volume are outside the 95% confidence band, indicating that things are getting worse year after year, generating an extra climate structural change. This is supported by our out-of-sample forecasts. Similar results are obtained for temperature. Apart from a few years, our in-sample predictions from 1980 to 2014 detect higher temperature values than the 95% confidence band of the model, and even after the late 1970s, the temperature was almost always higher than the temperature forecast, indicating that the structural changes in the model of temperature are still present after 1980, which is consistent with the global warming generated by GHG. This is also supported by our out-of-sample temperature forecasts. We have found that if the current trend of climate change continues, then global sea ice will disappear around 2077 with a mean $\pm$ 2 standard deviation interval forecast [2067, 2088].

Acknowledgments

Computer codes are available from the authors of this paper upon request. Álvaro Escribano acknowledges funding from Ministerio de Economía, Industria y Competitividad (ECO2016-00105-001 and MDM 2014-0431), Comunidad de Madrid (MadEco-CM S2015/HUM-3444), and Agencia Estatal de Investigación (2019/00419/001). The authors declare no conflict of interest.

References

Ahn, J., Hong, S., Cho, J., Lee, Y.-W., Lee, H., 2014. Statistical modeling of sea ice concentration using satellite imagery and climate reanalysis data in the Barents and Kara Seas, 1979-2012. Remote Sensing 6 (6), 5520-5540. doi:10.3390/rs6065520.

Andersson, T.R., Hosking, J.S., Pérez-Ortiz, M. Paige, B., Elliott, A., Russell, C., Law, S., Jones, D.C., Wilkinson, J., Phillips, T., Byrne, J. Tietsche, S., Sarojini, B.B., Blanchard-Wrigglesworth, E., Aksenov,

Y., Downie R., Shuckburgh, E., 2021. Seasonal Arctic sea ice forecasting with probabilistic deep learning. Nature Communications 12, 5124. doi:10.1038/s41467-021-25257-4.

Ayala, A., Blazsek, S., Escribano, A., 2022. Anticipating extreme losses using score-driven shape filters. Studies in Nonlinear Dynamics & Econometrics. doi:10.1515/snde-2021-0102.

Blanchard-Wrigglesworth, E., Barthelemy, A., Chevallier, M., Cullather, R., Fuckar, N., Massonnet, F., Posey, P., Wang, W., Zhang, J., Ardilouze, C., Bitz, C.M., Vernieres, G., Wallcraft S., Wang, M., 2017. Multi-model seasonal forecast of Arctic sea-ice: forecast uncertainty at pan-Arctic and regional scales. Climate Dynamics 49, 1399–1410. doi:10.1007/s00382-016-3388-9.

Blanchard-Wrigglesworth, E., Cullather, R. I., Wang, W., Zhang, J., Bitz, C. M., 2015. Model forecast skill and sensitivity to initial conditions in the seasonal Sea Ice Outlook. Geophysical Research Letters 42 (19), 8042–8048. doi:10.1002/2015GL065860.

Blasques, F., Koopman, S.J., Lucas, A., 2015. Information-theoretic optimality of observation-driven time series models for continuous responses. Biometrika 102 (2), 325–343. doi:10.1093/biomet/asu076.

Blasques, F., van Brummelen, J., Koopman, S.J., Lucas, A., 2022. Maximum likelihood estimation for score-driven models. Journal of Econometrics 227 (2), 325–346. doi:10.1016/j.jeconom.2021.06.003.

Blazsek, S., Ayala, A., Licht, A., 2022. Signal smoothing for score-driven models: a linear approach. Communications in Statistics - Simulation and Computation. doi:10.1080/03610918.2022.2032165.

Blazsek, S., Escribano, A., 2016a. Patent propensity, R&D and market competition: dynamic spillovers of innovation leaders and followers. Journal of Econometrics 191 (1), 145–163. doi:10.1016/j.jeconom.2015.10.005.

Blazsek, S., Escribano, A., 2016b. Score-driven dynamic patent count panel data models. Economics Letters 149 (C), 116–119. doi:10.1016/j.econlet.2016.10.026.

Blazsek, S., Escribano, A., 2022. Robust estimation and forecasting of climate change using score-driven ice-age models. Econometrics (Special Issue: Econometric Analysis of Climate Change) 10 (1). doi:10.3390/econometrics10010009.

Blazsek, S., Escribano, A., 2023. Score-driven threshold ice-age models: Benchmark models for long-run climate forecasts. Energy Economics 118, 106522. doi:10.1016/j.eneco.2023.106522.

Boé, J., Hall, A., Qu, X., 2009. September sea-ice cover in the Arctic Ocean projected to vanish by 2100. Nature Geoscience 2 (5), 341–343. doi:10.1038/ngeo467.

Bollerslev, T., 1986. Generalized autoregressive conditional heteroskedasticity. Journal of Econometrics 31 (3), 307–327. doi:10.1016/0304-4076(86)90063-1.

Box, G.E.P., Jenkins, G.M., 1970. Time Series Analysis, Forecasting, and Control. Holden-Day, San Francisco, US.

Brennan, M. K., Hakim, G. J., Blanchard-Wrigglesworth, E., 2023. Monthly Arctic sea-ice prediction with a Linear Inverse Model. Geophysical Research Letters 50 (7), e2022GL101656. doi:10.1029/2022GL101656.

Castle, J., Hendry, D.F., 2020. Climate Econometrics: An Overview. Foundations and Trends in Econometrics, vol. 10 (3–4), 145–322. doi:10.1561/0800000037.

Cox, D.R. 1981. Statistical analysis of time series: some recent developments. Scandinavian Journal of Statistics 8 (2), 93–115. https://www.jstor.org/stable/i412423.

Creal, D., Koopman, S.J., Lucas, A., 2008. A general framework for observation driven time-varying parameter models. Tinbergen Institute Discussion Paper 08-108/4. https://papers.tinbergen.nl/08108.pdf.

Diebold, F. X., Rudebusch, G. D., Göbel, M., Goulet Coulombe, P., Zhang, B. 2022. When will Arctic ice disappear? Projections of area, extent, thickness, and volume. NBER Working Paper No. 30732. http://www.nber.org/papers/w30732.

Docquier, D., Koenigk, T., 2021. Observation-based selection of climate models projects Arctic ice-free summers around 2035. Communications Earth & Environment 2 (1), 144. doi:10.1038/s43247-021-00214-7.

Engle, R.F., 1982. Autoregressive conditional heteroscedasticity with estimates of the variance of United Kingdom inflation. Econometrica 50 (4), 987–1007. doi:10.2307/1912773.

Escanciano, C., Lobato, I. N., 2009. An automatic Portmanteau test for serial correlation. Journal of Econometrics 151 (2), 140-149. doi:10.1016/j.jeconom.2009.03.001.

Everitt, B.S., 1993. Cluster Analysis, 3rd edition. E. Arnold, London, UK; Halsted Press, New York, US.

Eyring, V., Bony, S., Meehl, G.A., Senior, C.A., Stevens, B., Stouffer, R.J., Taylor, K.E., 2016. Overview of the Coupled Model Intercomparison Project Phase 6 (CMIP6) experimental design and organization. Geoscientific Model Development 9 (5), 1937–1958. doi:10.5194/gmd-9-1937-2016.

Guarino, M.V., Sime, L. C., Schröeder, D., Malmierca-Vallet, I., Rosenblum, E., Ringer, M., Ridley, J., Feltham, D., Bitz, C., Steig, E. J., Wolff, E., Stroeve, J., Sellar, A., 2020. Sea-ice-free Arctic during the last interglacial supports fast future loss. Nature Climate Change 10, 928–932. doi:10.1038/s41558-020-0865-2.

Harvey, A.C., 2013. Dynamic Models for Volatility and Heavy Tails: With Applications to Financial and Economic Time Series, Econometric Society Monographs. Cambridge University Press, Cambridge, UK.

Harvey, A.C., Chakravarty, T., 2008. Beta-t-(E)GARCH. Cambridge working papers in Economics 0840, Faculty of Economics, University of Cambridge, Cambridge. https://www.repository.cam.ac.uk/handle/1810/229418.

Holland, M.M., Bitz, C.M., Tremblay, B., 2006. Future abrupt reductions in the summer Arctic sea ice. Geophysical Research Letters 33 (23), L23503. doi:10.1029/2006GL028024.

IPCC, 2014. Climate Change 2014: Synthesis Report. Contribution of Working Groups I, II and III to the Fifth Assessment Report of the Intergovernmental Panel on Climate Change. Core Writing Team, R.K. Pachauri and L.A. Meyer (eds.). IPCC, Geneva, Switzerland.

IPCC, 2021. Climate Change 2021: The Physical Science Basis. Contribution of Working Group I to the Sixth Assessment Report of the Intergovernmental Panel on Climate Change. Masson-Delmotte, V., P. Zhai, A. Pirani, S.L. Connors, C. Péan, S. Berger, N. Caud, Y. Chen, L. Goldfarb, M.I. Gomis, M. Huang, K. Leitzell, E. Lonnoy, J.B.R. Matthews, T.K. Maycock, T. Waterfield, O. Yelekçi, R. Yu, and B. Zhou (eds.), Cambridge University Press, Cambridge, UK and New York, NY, US. doi:10.1017/9781009157896.

Jarque, C.M., Bera, A.K., 1980. Efficient tests for normality, homoscedasticity and serial dependence of regression residuals. Economics Letters 6 (3), 255–259. doi:10.1016/0165-1765(80)90024-5.

Jouzel, J., Masson-Delmotte, V., Cattani, O., Dreyfus, G., Falourd, S., Hoffmann, G.E., 2007. Orbital and millennial Antarctic climate variability over the past 800,000 years. Science 317, 793–797. doi:10.1126/science.1141038.

Jungclaus, J.H., Bard, E., Baroni, M., Braconnot, P., Cao, J., Chini, L.P., Egorova, T., Evans, M., González-Rouco, J.F., Goosse, H., Hurtt, G.C., Joos, F., Kaplan, J.O., Khodri, M., Klein Goldewijk, K., Krivova, N., LeGrande, A.N., Lorenz, S.J., Luterbacher, J., Man, W., Maycock, A.C., Meinshausen, M., Moberg, A., Muscheler, R., Nehrbass-Ahles, C., Otto-Bliesner, B.I., Phipps, S.J., Pongratz, J., Rozanov, E., Schmidt, G.A., Schmidt, H., Schmutz, W., Schurer, A., Shapiro, A.I., Sigl, M., Smerdon, J.E., Solanki, S.K., Timmreck, C., Toohey, M., Usoskin, I.G., Wagner, S., Wu, C.-J., Yeo, K.L., Zanchettin, D., Zhang, Q., and Zorita, E., 2017. The PMIP4 contribution to CMIP6 – Part 3: The last millennium, scientific objective, and experimental design for the PMIP4 past1000 simulations, Geoscientific Model Development 10 (11), 4005–4033. doi:10.5194/gmd-10-4005-2017.

Lauria, C. S. A. 2021. On the Optimality of Score-Driven Models. Doctoral Thesis, University of Bologna. http://amsdottorato.unibo.it/9627/1/Christopher_Lauria_tesi.pdf.

Lisiecki, L.E., Raymo, M.E., 2005. A Pliocene-Pleistocene stack of 57 globally distributed Benthic δ^{18}O records. Paleoceanography 20 (1). doi:10.1029/2004PA001071.

Ljung, G.M., Box, G.E.P., 1978. On a measure of lack of fit in time-series models. Biometrika 65 (2), 297–303. doi:10.1093/biomet/65.2.297.

Lüthi, D., Le Floch, M., Bereiter, B., Blunier, T., Barnola, J.-M., Steigenhaler, U., Raynaud, D., Jouzel, J., Fischer, H., Kawamura, K., Stocker, T.F., 2008. High-resolution carbon dioxide concentration record 650,000-800,000 years before present. Nature 453. doi:10.1038/nature06949.

Meinshausen, M., Vogel, E., Nauels, A., Lorbacher, K., Meinshausen, N., Etheridge, D.M., Fraser, P.J., Montzka, S.A., Rayner, P.J., Trudinger, C.M., Krummel, P.B., Beyerle, U., Canadell, J.G., Daniel, J.S., Enting, I.G., Law, R.M., Lunder, C.R., O'Doherty, S., Prinn, R.G., Reimann, S., Rubino, M., Velders, G.J.M, Vollmer, M.K., Wang, R.H.J., Weiss, R. 2017. Historical greenhouse gas concentrations for climate change modelling (CMIP6). Geoscientific Model Development 10 (5), 2057–2116. doi:10.5194/gmd-10-2057-2017.

Melillo, J.M., T.C. Richmond, and G.W. Yohe (Eds.), 2014. Climate Change Impacts in the United States: The Third National Climate Assessment. U.S. Global Change Research Program. doi:10.7930/J0Z31WJ2.

Newey, W.K., West, K.D., 1987. A simple, positive semi-definite, heteroskedasticity and autocorrelation consistent covariance matrix. Econometrica 55 (3), 703–708. doi:10.2307/1913610.

O'Neill, B.C., Tebaldi, C., van Vuuren, D.P., Eyring, V., Friedlingstein, P., Hurtt, G., Knutti, R., Kriegler, E., Lamarque, J.-F., Lowe, J., Meehl, G.A., Moss, R., Riahi, K., Sanderson, B.M., 2016. The scenario model intercomparison project (ScenarioMIP) for CMIP6. Geoscientific Model Development 9 (9), 3461–3482. doi:10.5194/gmd-9-3461-2016.

USGCRP, 2018. Impacts, Risks, and Adaptation in the United States: Fourth National Climate Assessment, Volume II. Reidmiller, D.R., C.W. Avery, D.R. Easterling, K.E. Kunkel, K.L.M. Lewis, T.K. Maycock, and B.C. Stewart (eds.). U.S. Global Change Research Program, Washington, DC, USA. doi: 10.7930/NCA4.2018.

Ruddiman, W. 2005., Plows, Plagues and Petroleum: How Humans Took Control of the Climate. Princeton University Press, Princeton, US.

Stroeve, J., Hamilton, L. C., Bitz, C. M., and Blanchard-Wrigglesworth, E., 2014. Predicting September sea ice: Ensemble skill of the SEARCH. Sea ice outlook 2008-2013. Geophysical Research Letters 41 (7), 2411–2418. doi:10.1002/2014GL059388.

Stroeve, J.C., Kattsov, V., Barrett, A., Serreze, M., Pavlova, T., Holland, M., Meier, W.N., 2012. Trends in Arctic sea ice extent from CMIP5, CMIP3 and observations. Geophysical Research Letters 39 (16),

L16502.
doi:10.1029/2012GL052676.

Tiao, G.C., Tsay, R.S., 1989. Model specification in multivariate time series. Journal of the Royal Statistical Society 51 (2), 157–213. doi:10.1111/j.2517-6161.1989.tb01756.x.

Yukimoto, S., Koshiro, T., Kawai, H., Oshima, N., Yoshida, K., Urakawa, S., Tsujino, H., Deushi, M., Tanaka, T., Hosaka, M., Yoshimura, H., Shindo, E., Mizuta, R., Ishii, M., Obata, A., Adachi, Y., 2019. MRI MRI-ESM2.0 model output prepared for CMIP6 CMIP historical. Version 20230214. Earth System Grid Federation. doi:10.22033/ESGF/CMIP6.6842.

Yukimoto, S., Koshiro, T., Kawai, H., Oshima, N., Yoshida, K., Urakawa, S., Tsujino, H., Deushi, M., Tanaka, T., Hosaka, M., Yoshimura, H., Shindo, E., Mizuta, R., Ishii, M., Obata, A., Adachi, Y. 2020. MRI MRI-ESM2.0 model output prepared for CMIP6 PMIP past1000. Version 20230211. Earth System Grid Federation. doi:10.22033/ESGF/CMIP6.6866.

Wang, M., Overland, J.E., 2009. A sea ice free summer Arctic within 30 years? Geophysical Research Letters 36 (7), L07502. doi:10.1029/2009GL037820.

Wang, M., Overland, J.E., 2012. A sea ice free summer Arctic within 30 years: An update from CMIP5 models. Geophysical Research Letters 39 (18), L18501. doi:10.1029/2012GL052868.

Ward, J.H., 1963. Hierarchical grouping to optimize an objective function. Journal of the American Statistical Association 58 (301), 236–244. doi:10.1080/01621459.1963.10500845.

Wu, D., Tian, W., Lang, X., Mao, W., Zhang, J., 2023. Statistical modeling of Arctic sea ice concentrations for Northern Sea route shipping. Applied Sciences 13 (7), 4374. doi:10.3390/app13074374.

Table 1. Descriptive statistics.

(a). Long-run data	Ice_t	Temp_t	$\text{CO}_{2,t}$
Name of variable	Ice volume	Antarctic-based land surface temperature	Atmospheric CO_2 concentration
Data frequency	1 thousand years	1 thousand years	1 thousand years
Measurement	Based on the $\delta^{18}\text{O}$ proxy	1 unit = 1 °C	1 unit = 780 gigatonnes of CO_2
Data source	Lisiecki and Raymo (2005)	Jouzel et al. (2007)	Lüthi et al. (2008)
Start date	798 thousands years ago	798 thousands years ago	798 thousands years ago
End date	1 thousand years ago	1 thousand years ago	1 thousand years ago
Sample size	798	798	798
Minimum	3.1000	−10.2530	1.7269
Maximum	5.0800	3.7662	2.9500
Mean	4.1707	−5.2892	2.2382
Standard deviation	0.4467	2.9009	0.2546
Jarque–Bera test	21.7157***	68.9779***	33.5370***
(b). Short-run data	Ice_t	Temp_t	$\text{CO}_{2,t}$
Name of variable	Ice volume	Antarctic-based land surface temperature	Atmospheric CO_2 concentration
Data frequency	1 year	1 year	1 year
Measurement (after scaling to long-run data)	Based on the $\delta^{18}\text{O}$ proxy	1 unit = 1 °C	1 unit = 780 gigatonnes of CO_2
Data source	Yukimoto et al. (2019, 2020)	Yukimoto et al. (2019, 2020)	Meinshausen et al. (2017)
Start date	AD 850	AD 850	AD 850
End date	AD 2014	AD 2014	AD 2014
Sample size	1,165	1,165	1,165
Minimum	2.5833	−0.4521	2.7428
Maximum	4.4189	−0.4521	3.9468
Mean	3.3322	−0.4039	2.8355
Standard deviation	0.2870	0.0068	0.1662
Jarque–Bera test	67.7071***	1.9079	19174.3000***
(c). Signal smoothing parameter estimates	Ice_t	Temp_t	$\text{CO}_{2,t}$
ϕ	0.8495***(0.0180)	0.9397***(0.0531)	NA
ψ	1.0640***(0.0428)	0.1226**(0.0517)	
λ	−2.0214***(0.0229)	−5.0566***(0.0266)	
ν	51.3715*(28.6780)	83.4550(113.2174)	
(d). Descriptive statistics for smoothed signals	Ice_t	Temp_t	$\text{CO}_{2,t}$
Start date	AD 850	AD 850	NA
End date	AD 2014	AD 2014	
Sample size	1,165	1,165	
Minimum	2.7082	−0.4321	
Maximum	4.3087	−0.4198	
Mean	3.3322	−0.4250	
Standard deviation	0.2582	0.0022	
Jarque–Bera test	99.1103***	171.4070***	

Notes: Anno Domini (AD); not available (NA). Standard errors are in parentheses. ***, **, and * indicate significance at the 1%, 5%, and 10% levels, respectively.

Table 2. In-sample estimates for the linear trend and score-driven climate models with two structural changes from 850 to 2014.

(a). Parameter estimates for linear trend model with two structural changes			
Global sea ice volume Ice_t		Antarctic-based land surface temperature Temp_t	
$\alpha(1)$	$3.2204^{***}(0.0330)$	$\alpha(1)$	$-0.4251^{***}(0.0005)$
$\beta(1)$	$0.0002^{**}(0.0001)$	$\beta(1)$	$0.0000(0.0000)$
$\alpha(2)$	$3.6281^{***}(0.1048)$	$\alpha(2)$	$-0.4335^{***}(0.0019)$
$\beta(2)$	$0.0014(0.0028)$	$\beta(2)$	$0.0001^{***}(0.0000)$
$\alpha(3)$	$4.0599^{***}(0.0258)$	$\alpha(3)$	$-0.4236^{***}(0.0027)$
$\beta(3)$	$-0.0418^{***}(0.0019)$	$\beta(3)$	$0.0001(0.0001)$
(b). Score-driven threshold climate model with two structural changes for Ice_t and Temp_t			
Parameter estimates		Model diagnostics	
$\Gamma_{1,1}(1)$	$0.8028^{***}(0.0200)$	LL	4.2570
$\Gamma_{2,2}(1)$	$0.8693^{***}(0.0404)$	AIC	-8.4727
$\Gamma_{1,1}(2)$	$0.7314^{***}(0.0970)$	BIC	-8.3684
$\Gamma_{2,2}(2)$	$0.4576(0.4219)$	HQC	-8.4334
$\Gamma_{1,1}(3)$	$0.2104(0.2816)$	Covariance stationarity	
$\Gamma_{2,2}(3)$	$-0.3505(0.2571)$	$C(1)$	0.8693
$\Psi_{1,1}(1)$	$1.0066^{***}(0.0400)$	$C(2)$	0.7314
$\Psi_{2,2}(1)$	$0.1599^{***}(0.0252)$	$C(3)$	0.3505
$\Psi_{1,1}(2)$	$1.0860^{***}(0.1145)$	Escanciano–Lobato test (p-value)	
$\Psi_{2,2}(2)$	$0.2202^{*}(0.1312)$	$v_{1,t}$	0.8955(0.3440)
$\Psi_{1,1}(3)$	$0.6841^{***}(0.1991)$	$v_{2,t}$	1.7112(0.1908)
$\Psi_{2,2}(3)$	$0.5921^{***}(0.1929)$	$u_{1,t}$	0.7386(0.3901)
$\Omega_{1,1}(1)$	$0.1325^{***}(0.0028)$	$u_{2,t}$	1.6991(0.1924)
$\Omega_{1,2}(1)$	$-0.0012^{***}(0.0002)$	Ljung–Box test (p-value)	
$\Omega_{2,2}(1)$	$0.0061^{***}(0.0001)$	$v_{1,t}$	34.9696(0.4218)
$\Omega_{1,1}(2)$	$0.1354^{***}(0.0128)$	$v_{2,t}$	27.5782(0.7739)
$\Omega_{1,2}(2)$	$0.0004(0.0011)$	$u_{1,t}$	35.8501(0.3817)
$\Omega_{2,2}(2)$	$0.0067^{***}(0.0007)$	$u_{2,t}$	28.0749(0.7527)
$\Omega_{1,1}(3)$	$0.0826^{***}(0.0131)$		
$\Omega_{1,2}(3)$	$0.0008(0.0020)$		
$\Omega_{2,2}(3)$	$0.0060^{***}(0.0011)$		
ν	$75.8342^{***}(27.7938)$		
$\mu_{1,0}$	$0.2613(1.0451)$		
$\mu_{2,0}$	$0.0003(0.0039)$		

Notes: Log-likelihood (LL); Akaike information criterion (AIC); Bayesian information criterion (BIC); Hannan–Quinn criterion (HQC). $C_i < 1$ indicates covariance stationarity for sub-period i, where $i = 1, 2, 3$ indicate the periods of 850 to 1906, 1907 to 1979, and 1980 to 2014, respectively. For the parameter estimates in (a) and (b), standard errors are in parentheses. The Escanciano–Lobato and Ljung–Box (LB) statistics (p-values are in parentheses) use the lag-order $\sqrt{T}$. For the linear trend model with two structural changes, we present OLS-HAC (ordinary least squares; heteroskedasticity and autocorrelation consistent) standard errors. For the score-driven climate model, we present inverse-information matrix-based standard errors. *, **, and *** indicate parameter significance at the 10%, 5%, and 1% levels, respectively.

Table 3. In-sample estimates for the linear trend and score-driven climate models with one structural change from 850 to 1979.

(a). Parameter estimates for linear trend model with one structural change			
Global ice volume Ice_t		Antarctic-based land surface temperature Temp_t	
$\alpha(1)$	$3.2204^{***}(0.0330)$	$\alpha(1)$	$-0.4251^{***}(0.0005)$
$\beta(1)$	$0.0002^{***}(0.0001)$	$\beta(1)$	$0.0000^{***}(0.0000)$
$\alpha(2)$	$3.6281^{**}(0.1048)$	$\alpha(2)$	$-0.4335(0.0019)$
$\beta(2)$	$0.0014(0.0028)$	$\beta(2)$	$0.0001^{***}(0.0000)$
(b). Score-driven threshold climate model with one structural change for Ice_t and Temp_t			
Parameter estimates		Model diagnostics	
$\Gamma_{1,1}(1)$	$0.8028^{***}(0.0200)$	LL	4.2415
$\Gamma_{2,2}(1)$	$0.8692^{***}(0.0404)$	AIC	-8.4529
$\Gamma_{1,1}(2)$	$0.7301^{***}(0.0973)$	BIC	-8.3772
$\Gamma_{2,2}(2)$	$0.4560(0.4330)$	HQC	-8.4243
$\Psi_{1,1}(1)$	$1.0100^{***}(0.0403)$	Covariance stationarity	
$\Psi_{2,2}(1)$	$0.1604^{***}(0.0253)$	$C(1)$	0.8692
$\Psi_{1,1}(2)$	$1.0866^{***}(0.1150)$	$C(2)$	0.7301
$\Psi_{2,2}(2)$	$0.2111(0.1353)$	Escanciano–Lobato test (p-value)	
$\Omega_{1,1}(1)$	$0.1324^{***}(0.0029)$	$v_{1,t}$	$0.8783(0.3487)$
$\Omega_{1,2}(1)$	$-0.0012^{***}(0.0002)$	$v_{2,t}$	$1.8490(0.1739)$
$\Omega_{2,2}(1)$	$0.0061^{***}(0.0001)$	$u_{1,t}$	$0.6986(0.4033)$
$\Omega_{1,1}(2)$	$0.1353^{***}(0.0128)$	$u_{2,t}$	$1.8339(0.1757)$
$\Omega_{1,2}(2)$	$0.0004(0.0011)$	Ljung–Box test (p-value)	
$\Omega_{2,2}(2)$	$0.0067^{***}(0.0007)$	$v_{1,t}$	$35.0196(0.4195)$
ν	$71.3960^{***}(25.2246)$	$v_{2,t}$	$27.7886(0.7650)$
$\mu_{1,0}$	$0.2621(1.0115)$	$u_{1,t}$	$35.9678(0.3765)$
$\mu_{2,0}$	$0.0004(0.0039)$	$u_{2,t}$	$28.3486(0.7406)$

Notes: Log-likelihood (LL); Akaike information criterion (AIC); Bayesian information criterion (BIC); Hannan–Quinn criterion (HQC). $C_i < 1$ indicates covariance stationarity for sub-period i, where $i = 1, 2$ indicate the periods of 850 to 1906 and 1907 to 1979, respectively. For the parameter estimates, standard errors are in parentheses. The Escanciano–Lobato and Ljung–Box (LB) statistics (p-values are in parentheses) use the lag-order $\sqrt{T}$. For the linear trend model with one structural change, we present OLS-HAC (ordinary least squares; heteroskedasticity and autocorrelation consistent) standard errors. For the score-driven climate model, we present inverse-information matrix-based standard errors. ** and *** indicate parameter significance at the 5% and 1% levels, respectively.

(a). Global sea ice volume Ice_t from 798 thousand years ago to the year 2014.

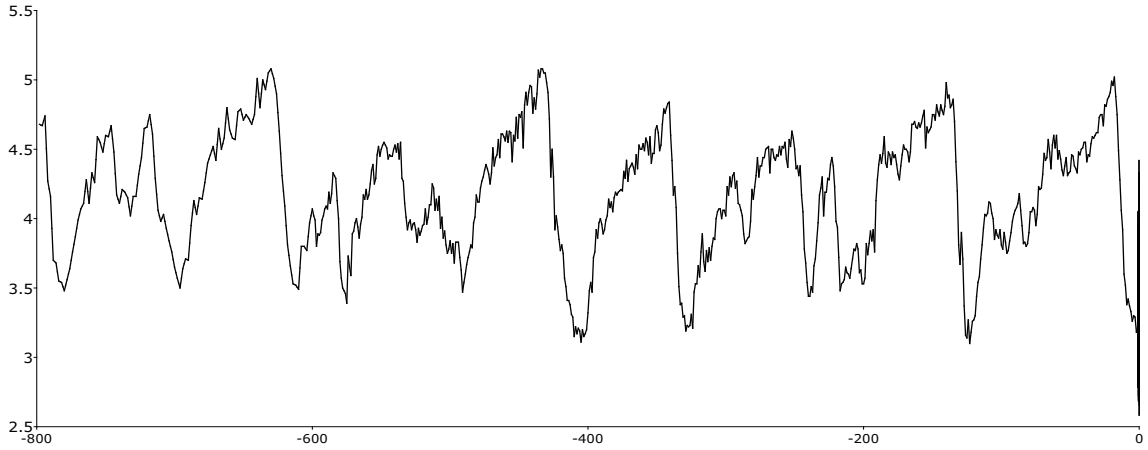

(b). Antarctic-based land surface temperature Temp_t from 798 thousand years ago to the year 2014.

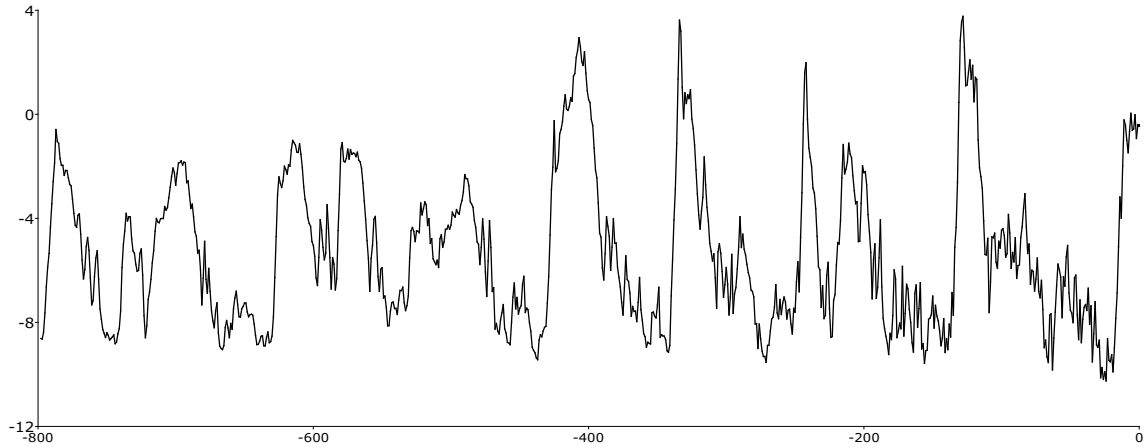

(c). Atmospheric CO_2 concentration $CO_{2,t}$ from 798 thousand years ago to the year 2014.

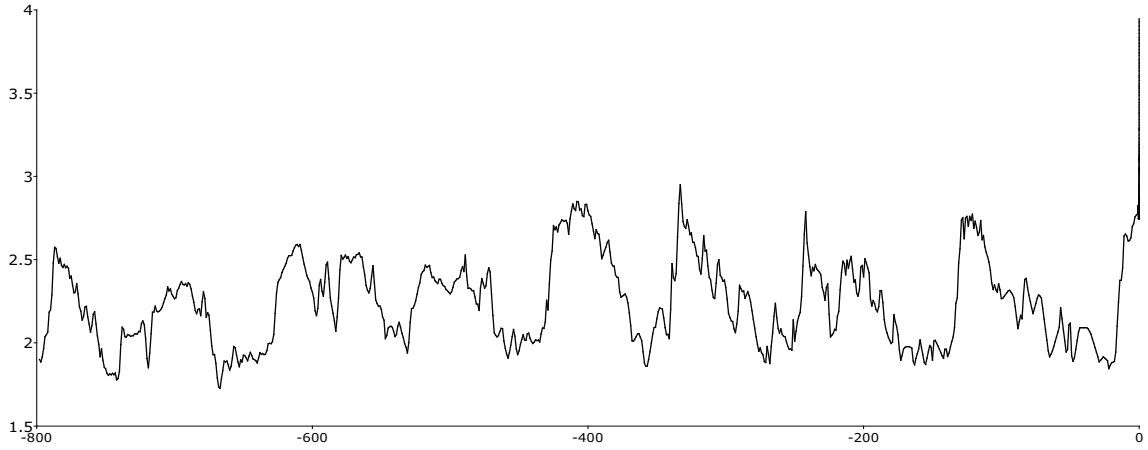

Fig. 1. Evolution of Ice_t, Temp_t, and $CO_{2,t}$ from 798 thousand years ago to 2014. *Notes:* On the x-axis, 1 unit = 1 thousand years. On the y-axis, (a) is based on the δ^{18}O proxy; (b) is 1 unit = 1 °C; (c) is 1 unit = 780 gigatonnes of CO_2. *Source of data:* Lisiecki and Raymo (2005), Jouzel et al. (2007), Lüthi et al. (2008), Yukimoto et al. (2019, 2020), and Meinshausen et al. (2017).

(a). Global sea ice volume Ice_t from 798 thousand years ago to the year 2114.

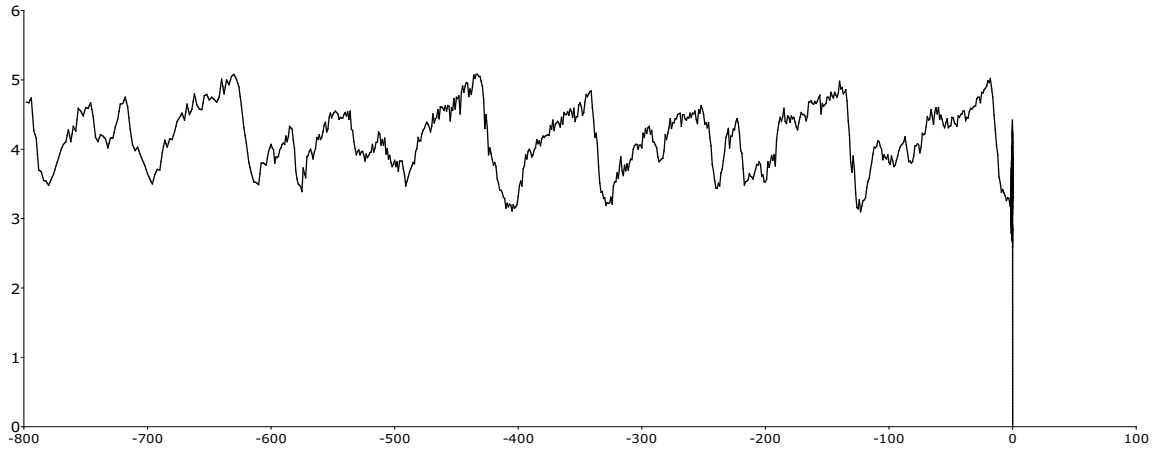

(b). Antarctic-based land surface temperature Temp_t from 798 thousand years ago to the year 2114.

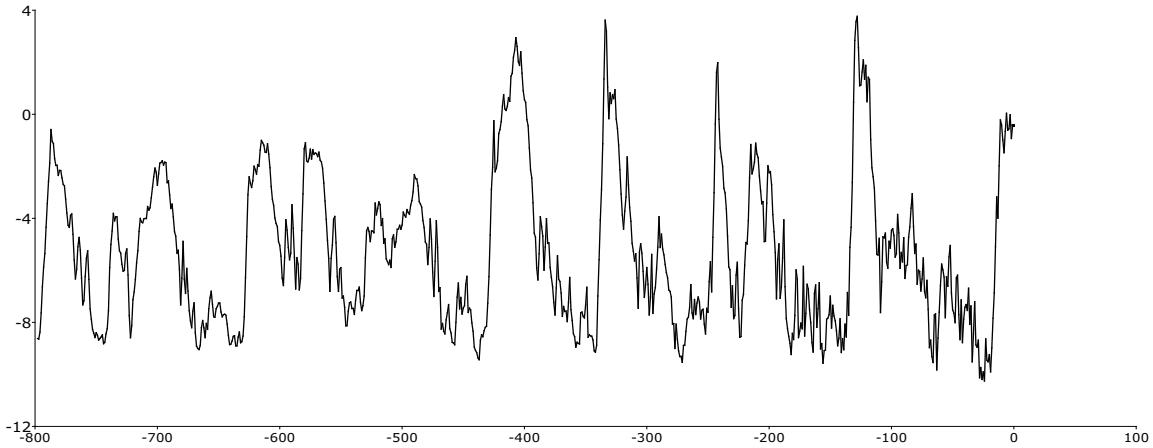

Fig. 2. Evolution and forecasts of Ice_t and Temp_t from 798 thousand years ago to the year 2114. *Notes:* For the period of 2015 to 2114, we use the forecasts of the score-driven climate model of the present paper. On the x-axis, 1 unit = 1 thousand years. On the y-axis, (a) is based on the δ^{18}O proxy; (b) is 1 unit = 1 °C. *Source of data:* Lisiecki and Raymo (2005), Jouzel et al. (2007), Lüthi et al. (2008), Yukimoto et al. (2019, 2020), and Meinshausen et al. (2017).

(a). Global sea ice volume Ice_t for the period of 850 to 2014.

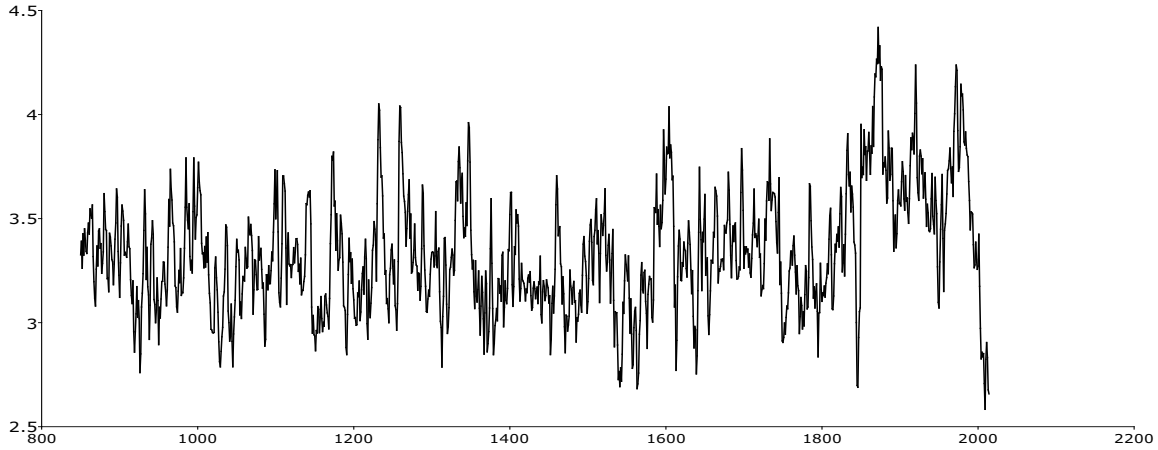

(b). Antarctic-based land surface temperature Temp_t for the period of 850 to 2014.

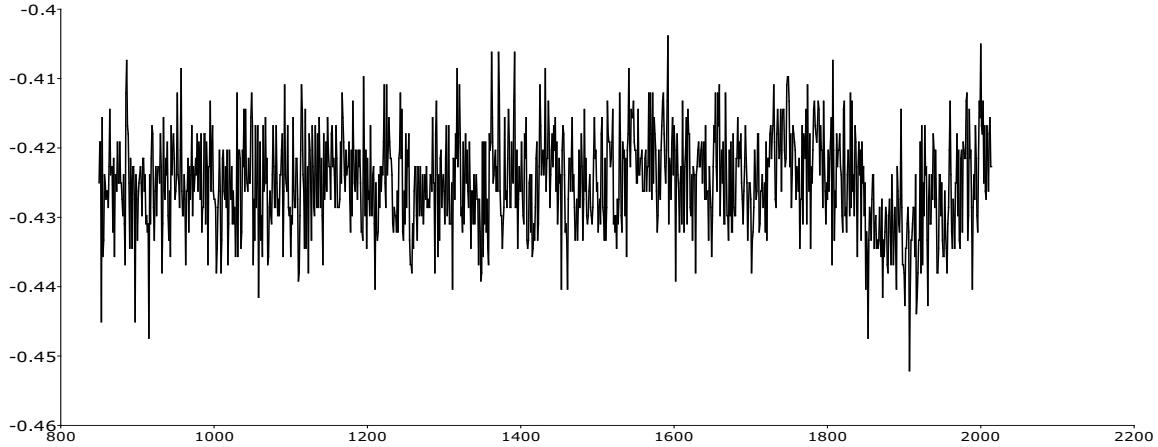

(c). Atmospheric CO_2 concentration $CO_{2,t}$ for the period of 850 to 2014.

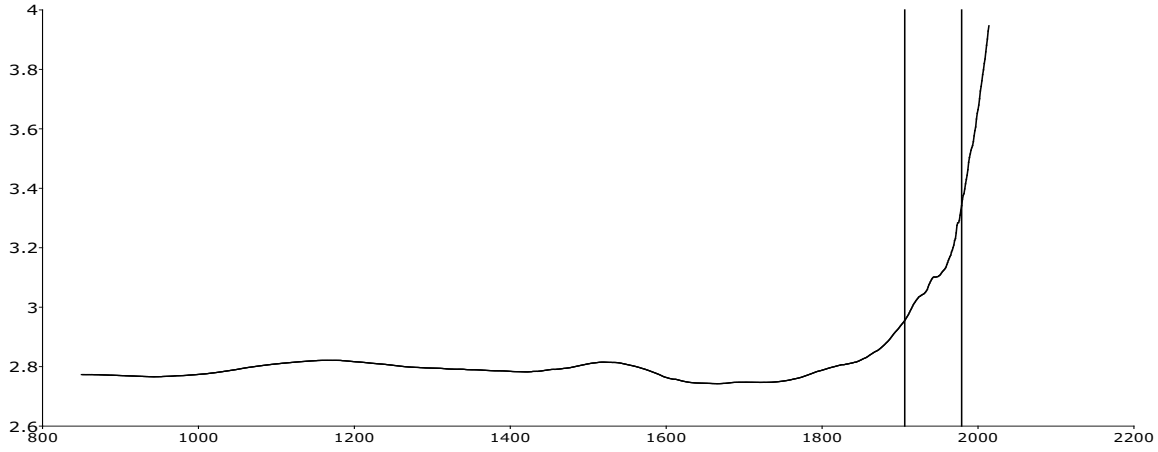

Fig. 3. Evolution of Ice_t, Temp_t, and $CO_{2,t}$ for the period of 850 to 2014. *Notes:* On the x-axis, 1 unit = 1 year. On the y-axis, (a) is based on the δ^{18}O proxy; (b) is 1 unit = 1 °C; (c) is 1 unit = 780 gigatonnes of CO_2. The vertical lines in Fig. 3(c) indicate the period breakpoints 1906 and 1979. *Source of data:* Yukimoto et al. (2019, 2020) and Meinshausen et al. (2017).

(a). Global sea ice volume (black) and its smoothed estimate (red) for the period of 850 to 2014.

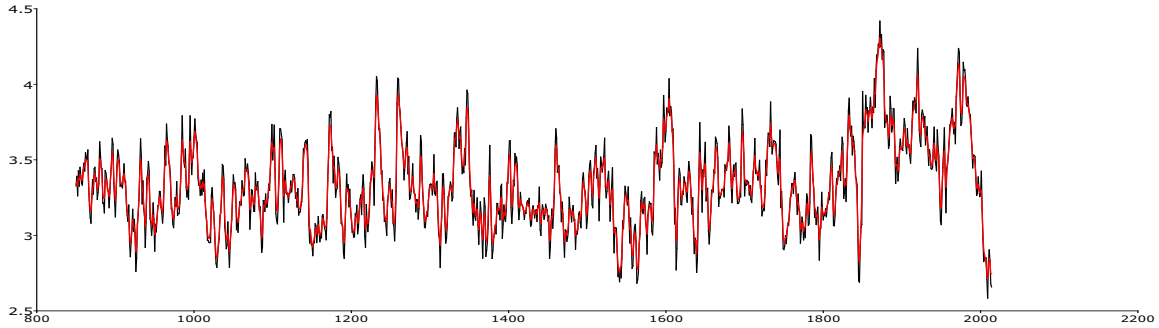

(b). Antarctic-based land surface temperature (black) and its smoothed estimate (red) for the period of 850 to 2014.

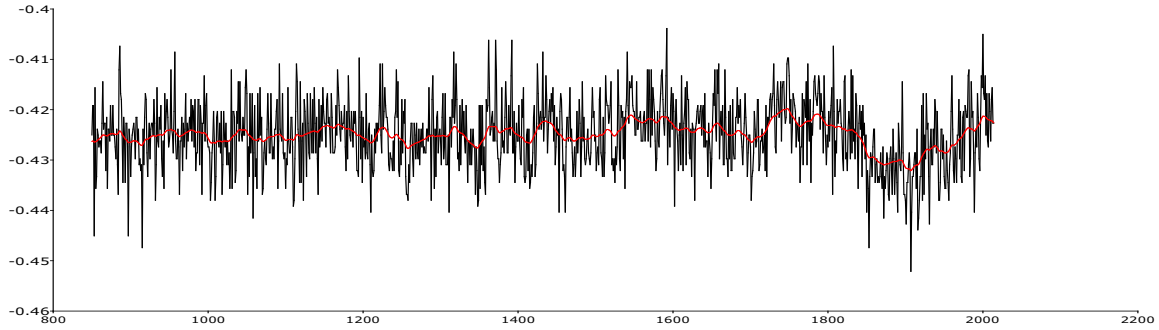

(c). $\mu_{\text{Ice},t}$, score-driven filter for global sea ice volume for the period of 850 to 2014.

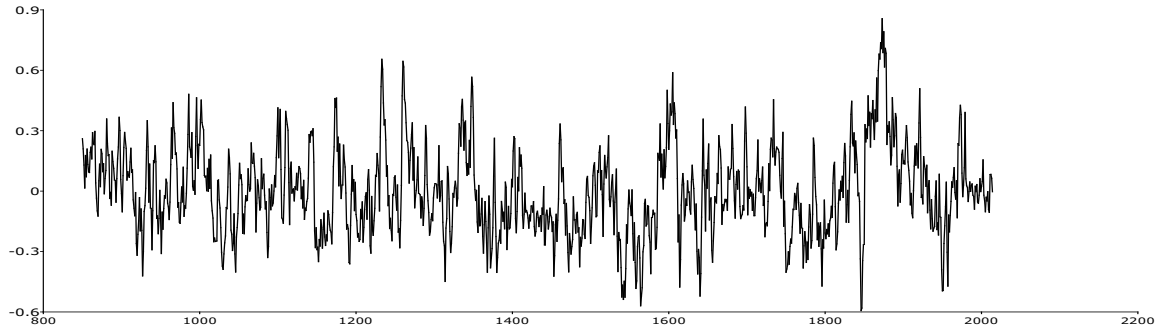

(d). $\mu_{\text{Temp},t}$ score-driven filter for Antarctic-based land surface temperature for the period of 850 to 2014.

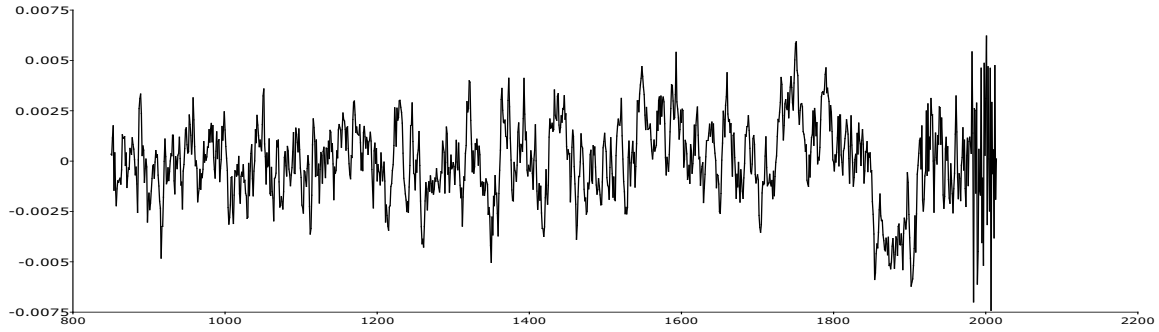

Fig. 4. Evolution of Ice_t, Temp_t, their smoothed estimates and evolution of $\mu_{\text{Ice},t}$ and $\mu_{\text{Temp},t}$ for the period of 850 to 2014. *Notes:* On the x-axis, 1 unit = 1 year. On the y-axis, (a) is based on the δ^{18}O proxy; (b) is 1 unit = 1 °C. *Source of data:* Lisiecki and Raymo (2005), Jouzel et al. (2007), Lüthi et al. (2008), Yukimoto et al. (2019, 2020), and Meinshausen et al. (2017).

(a). $u_{1,t}$ as a function of $\epsilon_{1,t}$ and $\epsilon_{2,t}$.

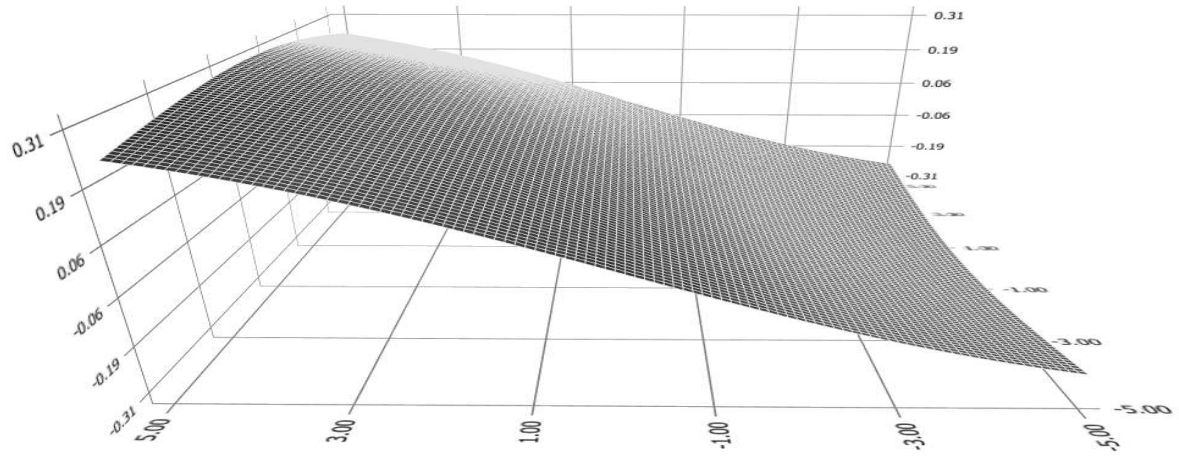

(b). $u_{2,t}$ as a function of $\epsilon_{1,t}$ and $\epsilon_{2,t}$.

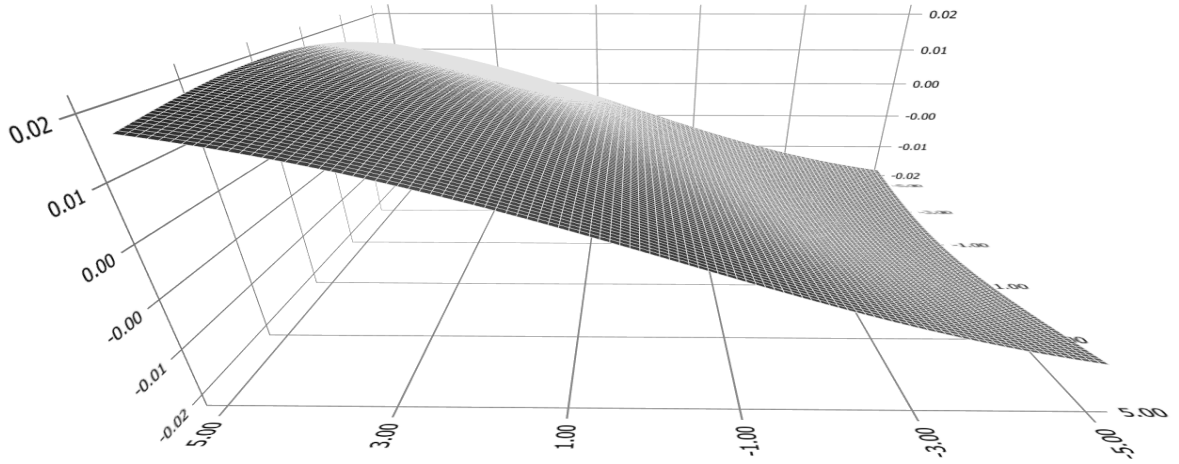

Fig. 5. Robustness of the scaled score function to extreme values. *Notes:* We present the estimates of the scaled score functions from 1980 to 2014. Notice the significant discounting of the extreme observations, even though the degrees of freedom parameter is relatively high, $\nu = 75.8342$.

(a). Error term $v_{\text{Ice},t}$ (black) and scaled score function $u_{\text{Ice},t}$ (red) for the period of 850 to 2014.

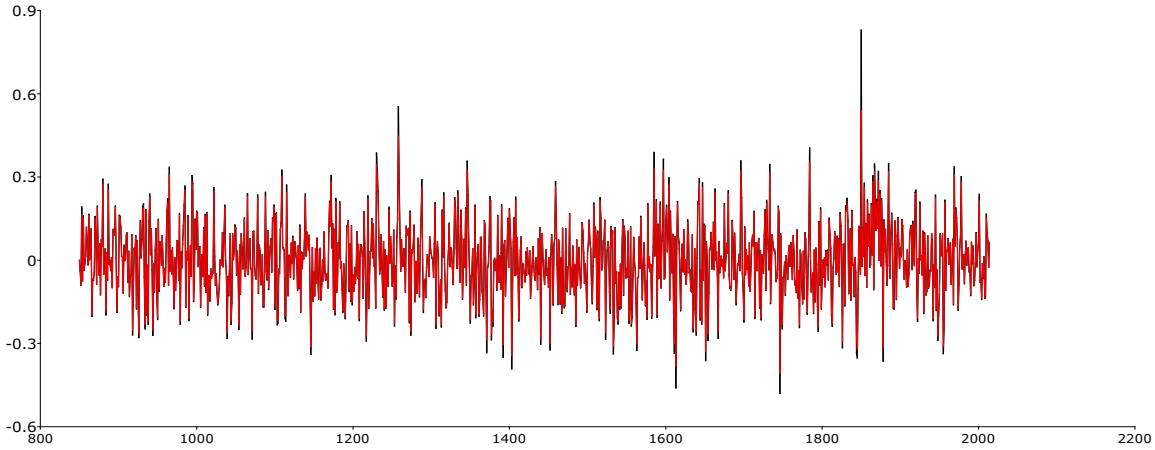

(a). Error term $v_{\text{Temp},t}$ (black) and scaled score function $u_{\text{Temp},t}$ (red) for the period of 850 to 2014.

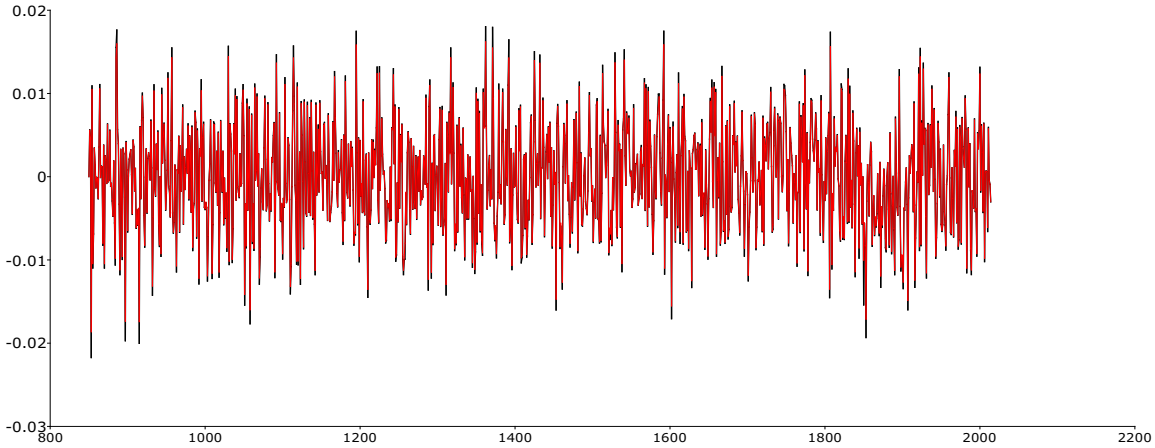

Fig. 6. Error terms $v_{\text{Ice},t}$ and $v_{\text{Temp},t}$ and scaled score functions $u_{\text{Ice},t}$, and $u_{\text{Temp},t}$ for the period of 850 to 2014.
Notes: On the x-axis, 1 unit = 1 year. On the y-axis, (a) is based on the δ^{18}O proxy; (b) is 1 unit = 1 °C.

(a). Global sea ice volume for the period of 1980 to 2014.

(b). Antarctic-based land surface temperature for the period of 1980 to 2014.

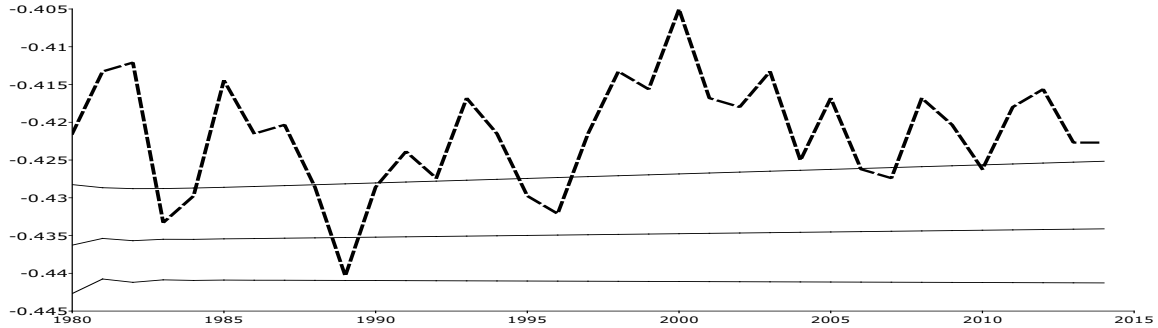

Fig. 7. Evolution and in-sample forecasts of Ice_t and Temp_t for the period of 1980 to 2014. *Notes:* For the in-sample forecasts, we use the one-regime and two-regime score-driven climate models of the present paper. The interval forecasts correspond to $\pm 2\sigma$ around the mean. On the x-axis, 1 unit = 1 year. On the y-axis, (a) is based on the δ^{18}O proxy; (b) is 1 unit = 1 °C. *Source of data:* Yukimoto et al. (2019, 2020) and Meinshausen et al. (2017).

(a). Global sea ice volume for the period of 850 to 2114.

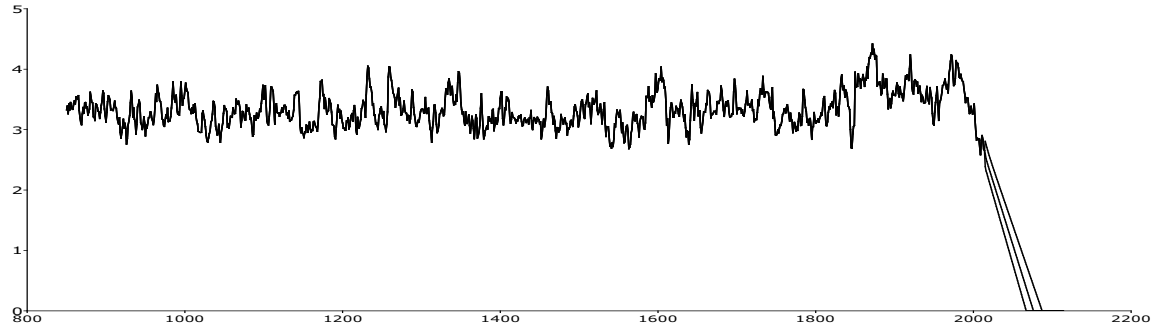

(b). Antarctic-based land surface temperature for the period of 850 to 2114.

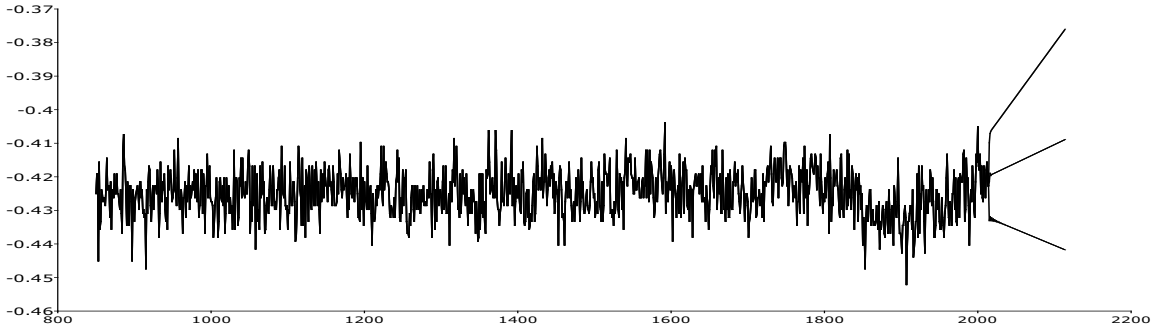

(c). Global sea ice volume for the period of 1980 to 2114.

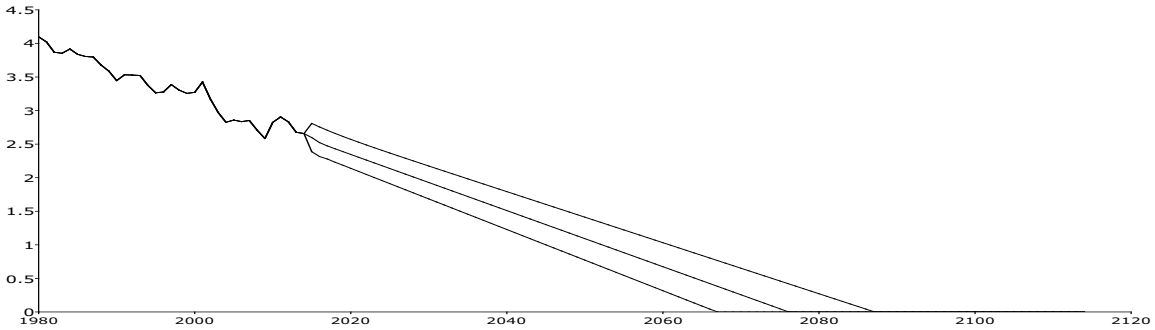

(d). Antarctic-based land surface temperature for the period of 1980 to 2114.

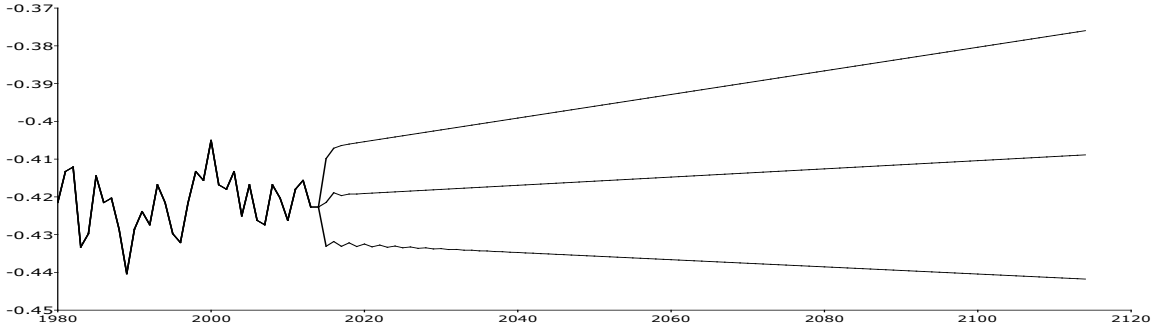

Fig. 8. Evolution and out-of-sample forecasts of Ice_t and Temp_t for the periods of 850 to 2114 and 1980 to 2114. *Notes:* For the period of 2015 to 2114, we use the forecasts of the score-driven climate model of the present paper. The interval forecasts correspond to $\pm 2\sigma$ around the mean. On the x-axis, 1 unit = 1 year. On the y-axis, (a) and (c) are based on the δ^{18}O proxy; (b) and (d) are 1 unit = 1 °C. *Source of data:* Yukimoto et al. (2019, 2020) and Meinshausen et al. (2017).